JOURNAL OF VIROLOGY, Oct. 2005, p. 12921–12933 Vol. 79, No. 20
0022-538X/05/$08.00+0 doi:10.1128/JVI.79.20.12921–12933.2005

T-Cell Tropism and the Role of ORF66 Protein in Pathogenesis of Varicella-Zoster Virus Infection

Anne Schaap,[1]* Jean-Francois Fortin,[2] Marvin Sommer,[1] Leigh Zerboni,[1] Shaye Stamatis,[1] Chia-Chi Ku,[1] Garry P. Nolan,[2] and Ann M. Arvin[1,2]

Departments of Pediatrics[1], and Microbiology and Immunology,[2] Stanford University School of Medicine, 300 Pasteur Dr., Stanford, California 94305-5208

Received 23 February 2005/Accepted 25 July 2005

The pathogenesis of varicella-zoster virus (VZV) involves a cell-associated viremia during which infectious virus is carried from sites of respiratory mucosal inoculation to the skin. We now demonstrate that VZV infection of T cells is associated with robust virion production and modulation of the apoptosis and interferon pathways within these cells. The VZV serine/threonine protein kinase encoded by ORF66 is essential for the efficient replication of VZV in T cells. Preventing ORF66 protein expression by stop codon insertion (pOka66S) impaired the growth of the parent Oka (pOka) strain in T cells in SCID-hu T-cell xenografts in vivo and reduced formation of VZV virions. The lack of ORF66 protein also increased the susceptibility of infected T cells to apoptosis and reduced the capacity of the virus to interfere with induction of the interferon (IFN) signaling pathway following exposure to IFN-γ. However, preventing ORF66 protein expression only slightly reduced growth in melanoma cells in culture and did not diminish virion formation in these cells. The pOka66S virus showed only a slight defect in growth in SCID-hu skin implants compared with intact pOka. These observations suggest that the ORF66 kinase plays a unique role during infection of T cells and supports VZV T-cell tropism by contributing to immune evasion and enhancing survival of infected T cells.

Varicella-zoster virus (VZV) is an alphaherpesvirus that causes chicken pox, or varicella, establishes lifelong latency in the sensory ganglia, and later reactivates to cause shingles, or herpes zoster. The pathogenesis of primary VZV infection is characterized by inoculation of respiratory mucosa, followed by a cell-associated viremia and a subsequent vesicular rash that develops 10 to 21 days after exposure (3). T cells appear to be a major target cell for VZV viremia. The virus infects primary human T cells in vitro and exhibits tropism for T cells in thymus/liver xenografts in the severe combined immunodeficiency (SCID)-hu mouse model in vivo (28, 35, 49). VZV alters cellular gene expression in T cells, as shown by down-regulation of major histocompatibility (MHC) class I protein expression and microarray analysis of gene transcription (1, 18). Importantly, T cells have the capacity to transport infectious VZV through the circulation, resulting in the formation of typical cutaneous lesions in SCID-hu skin xenografts (29). The goal of these experiments was to further investigate the T-cell tropism of VZV by examining virion formation, effects on apoptotic and interferon (IFN) pathways in human T cells, and the contributions of the ORF66 protein to these processes, based on previous evidence that preventing ORF66 protein expression decreased VZV virulence in T-cell xenografts in vivo (37).

The putative early gene ORF66 encodes a 47-kDa protein that localizes to both nuclei and cytoplasm of infected cells in vitro and is present in the VZV virion (22, 50). Sequence analysis has revealed that ORF66 is highly homologous to serine/threonine protein kinases in other alphaherpesviruses, including herpes simplex virus type 1 (HSV-1) U_S3, and shows similarity to the human serine/threonine kinase 9 and cyclin-dependent kinase 1 (22, 38, 50). VZV also encodes the ORF47 protein, which is related to the casein kinase II cellular proteins and is conserved in all herpesvirus subgroups. The ORF66 protein is dispensable for VZV replication in vitro, as shown by studies of ROKA66S, a recombinant virus derived from the vaccine strain of VZV (vOka), in which ORF66 translation was prevented by stop codon insertion (14). Replication of this vOka-derived ROKA66S mutant was not altered in skin xenografts when compared to vOka, but infection of T-cell xenografts was impaired substantially, suggesting that ORF66 may have a unique role in VZV T-cell tropism (37).

The ORF66 protein phosphorylates the major immediate-early transactivating protein encoded by ORF62/ORF71, designated the IE62 protein (32). By analogy with HSV U_S3, the ORF66 protein kinase probably has other substrates, including a number of viral and cellular targets (46). VZV ORF66 protein kinase is not necessary for the phosphorylation of other viral phosphoproteins, IE4, IE63, and gE, in vitro, implying that these proteins can be phosphorylated effectively by ORF47 protein or cellular kinases (14). As tegument components, ORF66 and ORF62 proteins are delivered simultaneously into the cytoplasm of the infected cell after uncoating (21, 22). Although ORF66 does not encode the predominant virion protein kinase activity, a 34% reduction in the total level of phosphorylation in virions that do not express ORF66 suggests that the gene contributes to virion-associated kinase activity (14, 22). Phosphorylation of IE62 by ORF66 is thought to mask the IE62 nuclear localization signal, causing nuclear exclusion of IE62 in the late stages of infection (22). The physical interaction between ORF66 and IE62 proteins may also con-

* Corresponding author. Mailing address: G312, Department of Pediatrics, Stanford University School of Medicine, 300 Pasteur Dr., Stanford, CA 94305-5208. Phone: (650) 725-6555. Fax: (650) 725-8040. E-mail: aschaap@stanford.edu.

tribute to tegument formation, though such an interaction has not yet been shown. However, the efficient replication of the ROKA66S mutant in cell culture suggests that ORF66 protein-mediated phosphorylation of the IE62 protein and potential ORF66-IE62 protein binding are not essential for VZV infectivity in vitro.

In addition to its kinase activity, HSV U_S3 has been found to have an important role in protecting infected cells from virus-induced apoptosis (8–11, 39, 40, 51). Whether ORF66 may also block apoptosis has not been explored. However, the potential of ORF66 protein to modulate cellular proteins is suggested by evidence of its contribution to the down-regulation of cell surface expression of MHC class I molecules in VZV-infected cells (1).

In previous work, Moffat et al. found that the tissue culture-passaged vOka virus was attenuated in its growth in skin xenografts but not in T-cell xenografts when compared with the low-passage clinical isolate, parent Oka virus (pOka) (36). As noted, evaluations of ORF66 function using the vOka-derived recombinant ROKA66S showed no incremental attenuation compared to vOka in skin xenografts (37). The current experiments to further analyze VZV T-cell tropism and the functions of ORF66 protein in VZV pathogenesis were done with VZV recombinants constructed from pOka cosmids (41). New and established assays were used to examine pOka infection of T cells and to evaluate the effects of deleting the ORF66 gene, preventing ORF66 translation, and inserting conservative alanine substitutions into consensus sites for ORF66 phosphorylation in the context of the pOka genome. pOka and pOka ORF66 mutants were evaluated for growth kinetics in vitro and in human T-cell and skin xenografts in vivo, for VZ virion formation, and for effects on apoptotic and interferon pathways in T cells.

MATERIALS AND METHODS

Generation of pOka recombinant viruses with mutations in ORF66. Recombinant viruses were generated using cosmids derived from pOka (41). The entire pOka genome is contained in four overlapping SuperCos 1 cosmid vectors (Stratagene, La Jolla, CA) designated pvFsp73 (pOka nucleotides [nt] 1 to 33128; Dumas nt 1 to 33211), pvSpe14 (pOka nt 21796 to 61868; Dumas nt 21875 to 62008), pvPme2 (pOka nt 53756 to 96035; Dumas nt 53877 to 96188), and pvSpe23 (pOka nt 94055 to 125123; Dumas nt 94208 to 124884). ORF66 is located in the unique short region in the cosmid pvSpe23 (Fig. 1). In order to make mutations in ORF66, the cosmid pvSpe23ΔAvr was digested with SacI, and the 6-kb SacI-SacI fragment was inserted into pBluescript KS(−) plasmid vector (Stratagene) to make pSac6A, containing open reading frames (ORFs) 64 to 69. Three individual mutations were made using the QuikChange site-directed mutagenesis kit XL (Stratagene): insertion of an early stop codon; substitution of Ser48, which is within a consensus sequence for phosphorylation by VZV ORF47; and substitution of Ser331 and Ser332, which are both within a consensus sequence for phosphorylation by cellular PKA or PAK2. The pOka66S mutant was made by introducing four stop codons into ORF66 at the 21st codon using the following oligonucleotide and its reverse complement: 5′-CGTGGCG CCATCTGATAATGACCGTCACATATTTAG-3′ (stop codons are underlined). The serine-to-alanine substitutions in putative phosphorylation sites, designated S48A and S331A, were constructed using oligonucleotides 5′-CCCGG CATAGAAGCTGAGGATGATCC-3′ and 5′-GGCAAAACGGGCTGCTCG AAAACCCGG-3′, respectively, and their reverse complements. The PCR primers were manufactured by OPERON Technologies, Inc. (Alameda, CA). The 4.5-kb AvrII/SgrAI fragments from these mutated plasmids replaced the original 4.5-kb AvrII/SgrAI fragment in pvSpe23ΔAvr.

Two independent deletions of the ORF66 gene were made by introducing an XbaI site by PCR over the start codon (pOka 113,140; Dumas 113,037), as well as at either codon 114,328 (Dumas 114,225) for a full deletion or 114,273 (Dumas 114,170) for a partial deletion. The primers used for the start codon were 5′-GCCATAGAAATCCAGATTGT-3′ and 5′-CAACGTCGTTCTAGATACT T-3′. The primers used at the 3′ end of ORF66 were 5′-AAATTCATCTAGA CTGTTAA-3′ and 5′-TATACGGGGACTTGTCTACC-3′ for the full deletion and 5′-CTCTGTTTTCTAGACTCTTCCCGATC-3′ and 5′-TATACGGGGAC TTGTCTACC-3′ for the partial deletion. Triple ligation into the AvrII and SgrAI sites of pvSpe23ΔAvr resulted in an XbaI site in place of the deleted ORF66 sequence (Spe23ΔORF66 [nt 1 to 1181] and Spe23ΔORF66 [nt 1 to 1133]).

Repaired cosmids, ΔORF66R and partialΔORF66R, were constructed by cloning the ORF66 gene, including the putative promoter region and the polyadenylation site, into a unique AvrII restriction site at nucleotide 112,956 (Dumas 112,854) in the cosmids Spe23ΔORF66 (nt 1 to 1181) and Spe23ΔORF66 (nt 1 to 1133). The ORF66 gene was amplified by PCR by using the oligonucleotides 5′-GCCCTCTTATCCTAGGATCAC-3′ and 5′-ACAATCCTAGGAAA ATGATCCC-3′ (pOka nt 113,022 and 114,499; Dumas nt 112,919 and 114,396) to introduce AvrII sites at each end. The amplified ORF66 gene was ligated into Spe23ΔORF66 (nt 1 to 1181) and Spe23ΔORF66 (nt 1 to 1133) at the AvrII site, and clones containing ORF66 in the native, 5′-to-3′ orientation (upper strand) were selected. The pvSpe23pΔORF66R cosmid generated the VZV strain pOka-pΔORF66R, which has a partial deletion of ORF66 and the intact ORF66 gene at the AvrII site.

The myc epitope was also inserted within the C terminus of ORF66, 6 nucleotides upstream of the ORF67 promoter sequence (29RE) and 32 nucleotides upstream of the ORF66 stop codon. Although the ORF67 coding region begins at nucleotide 114,599 in pOka (114,496 in Dumas), important promoter sequences begin at residue 114,292 in pOka (114,189 in Dumas) (13). The inserted myc tag sequence was 5′-GGCCCTTCGAACAAAAACTCATCTCAGAAGA GGATCTGAATATGCATACCGGTG-3′. The myc epitope and remaining C-terminal residues of ORF66 following the insertion are in frame, with the myc epitope between ORF66 amino acid residues P382 and D383.

Transfection, virus isolation, and growth kinetics. Recombinant viruses were isolated by transfection of human melanoma (MeWo) cells with mutated pvSpe23ΔAvr cosmid and the three intact cosmids, pFsp73, pSpe14, and pPme2, as described previously (31, 48). Melanoma cells were maintained in tissue culture medium (Mediatech, Washington, D.C.) supplemented with 10% fetal calf serum (Gemini Bio-Products, Woodland, CA), nonessential amino acids, and antibiotics. All mutations were sequenced to verify substitutions. DNA was isolated from melanoma cells with DNAzol reagent (GIBCO/BRL, Grand Island, NY) and from implant tissues using the DNeasy tissue kit (QIAGEN, Inc., Chatsworth, CA). PCR was performed using Elongase enzyme mix (GIBCO). Solubilized DNA was used as a template for PCR primers that annealed in the intergenic regions upstream and downstream of ORF66. PCR products were cloned into pCR4-TOPO (Invitrogen, Carlsbad, CA) and sequenced by the Stanford Protein and Nucleic Acid Facility or Sequetech Corp. (Mountain View, CA). Sequencing reactions were primed using the M13 primers contained in the PCR4-TOPO vector and custom primers within ORF66. Replication of pOka and pOka ORF66 mutants was assessed by infectious focus assay. Cells from three replicate wells were trypsinized on days 1 to 6 after inoculation, and the number of infectious foci was determined by titration on melanoma cell monolayers at each time point as described elsewhere (35, 37). Statistical comparisons were done using Student's *t* test.

ORF66 antibody and immunoblotting. Polyclonal anti-ORF66 protein antiserum was made by cloning nucleotides 1 to 570 or 774 to 1149 of ORF66 into pGEX-2T (Pharmacia Biotech, Milwaukee, WI) by PCR with primers containing BamHI and SmaI sites. Protein expression was induced, and the purified glutathione *S*-transferase fusion peptides were used for rabbit immunization (47). Rabbit immunization was performed at Josman, LLC (Napa, CA). Rabbit serum was collected before and after immunization and stored at −20°C. Immunoglobulin G (IgG) was isolated from the serum using an ImmunoPure (protein A) IgG purification column (Pierce, Rockford, IL). Purified IgG was preadsorbed overnight at 4°C with an equal volume of uninfected melanoma cell lysate, and anti-ORF66 IgG was used at 1:500.

Infected and uninfected melanoma cells were lysed with radioimmunoprecipitation assay buffer (50 mM Tris [pH 8], 150 mM NaCl, 1% IGEPAL CA-360 [Sigma, St. Louis, MO], 0.1% sodium dodecyl sulfate [SDS; Bio-Rad, Hercules, CA], 0.5% deoxycholic acid [Sigma]) containing a Complete Mini tablet (Roche, Inc.) in 1-ml volumes per T-75 flask and sonicated. Lysates were boiled in sample buffer and separated by SDS-polyacrylamide gel electrophoresis in 10% gels. Proteins were transferred to Immobilon-P (polyvinylidene difluoride) membranes (Millipore, Bedford, MA). The amount of total protein in 15 μl of each sample was equivalent as verified by Bradford assay (Bio-Rad) and amido black stain.

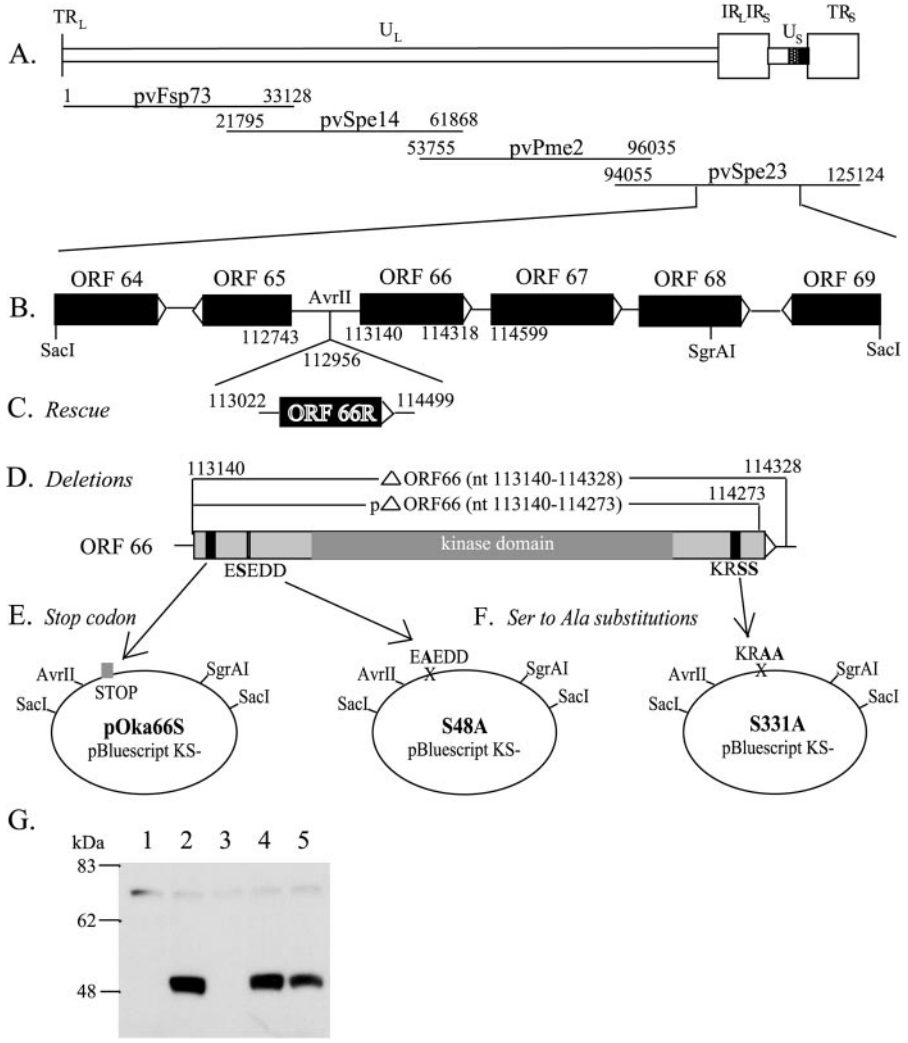

FIG. 1. Construction of cosmid vectors with mutations in VZV pOka ORF66. (A) Schematic diagram of the VZV genome with the location of ORF66 in the U_s region and the four overlapping segments of the VZV genome used to construct the VZV pOka cosmids. All coordinates given are for the pOka strain used to generate these cosmids; the equivalent coordinates for the Dumas sequence are given in Materials and Methods. (B) The 6.1-kb SacI-SacI fragment, subcloned from cosmid pvSpe23ΔAvr into pBluescript KS(−). (C) ORF66R, containing the ORF66 gene along with upstream and downstream elements, was inserted into the unique AvrII site to rescue lethal mutations. (D) Two ORF66 deletion mutants were made, removing all or most of the ORF66 sequence. (E) Four STOP codons were inserted at amino acid 21 of ORF66 to yield the ORF66S construct. (F) Two point mutations were made in putative phosphorylation sites: S48A and S331A. All mutations were reinserted into Spe23 via the 4.5-kb AvrII-SgrAI fragment. (G) Immunoblot analysis of lysate from uninfected melanoma (MeWo) cells (lane 1) or melanoma cells infected with pOka (lane 2), pOka66S (lane 3), pOka66S48A (lane 4), or pOka66S331A (lane 5). ORF66 is detected at approximately 48 kDa by ORF66-specific antibodies.

Infection of human xenografts in SCID-hu mice. T-cell or skin xenografts were engrafted in male homozygous *C.B-17*$^{scid/scid}$ mice (35) using human fetal tissues obtained with informed consent according to federal and state regulations. Animals were cared for according to guidelines of the Animal Welfare Act PL 94-279 and the Stanford University Administrative Panel on Laboratory Animal Care. VZV recombinant viruses were isolated in human melanoma cells, passed three times onto human embryonic lung fibroblasts (HEL), and stored at −80°C in tissue culture medium supplemented with 10% fetal calf serum, antibiotics, and 10% dimethyl sulfoxide. Infectious virus titers were determined for each inoculum at the time the implants were injected. Skin xenografts were harvested at 14, 21, and 28 days after inoculation. T-cell xenografts were harvested at 7, 14, and 21 days after inoculation or mock infection. Tissues were analyzed by infectious focus assay, PCR/sequencing to verify expected mutations, and immunohistochemistry. Gradient-purified T cells from xenografts were analyzed by fluorescence-activated cell sorter (FACS) using aliquots of approximately 10^6 cells that were washed and resuspended in 100 μl of FACS staining buffer (phosphate-buffered saline [PBS] with 1% fetal calf serum–0.2% sodium azide). The cells were incubated with human VZV immune or nonimmune polyclonal IgG on ice for 30 minutes, washed in staining buffer, and incubated with goat anti-human fluorescein isothiocyanate (FITC)-conjugated $F(ab')_2$ fragments (Caltag, Inc., Burlingame, CA) and mouse monoclonal anti-CD3–phycoerythrin (Caltag) on ice for another 30 min to detect VZV antigens and T-cell markers. The cells were then washed, resuspended in staining buffer, and analyzed on a FACSCalibur (Becton Dickinson, Inc.). As negative controls, cells were incubated with the appropriate isotype control antibodies.

Confocal microscopy for VZV protein expression. At 72 h after infection, VZV-infected monolayers were fixed with 2% paraformaldehyde, permeabilized with 0.1% Triton X-100, and washed with PBS (0.01 M; pH 7.4). Cells were blocked overnight at 4°C with PBS containing 0.2% bovine serum albumin and 10% normal goat serum. After washing with PBS, cells were then incubated for 1 hour at 37°C with murine anti-IE62 monoclonal antibody (Chemicon, Temecula, CA) and rabbit anti-ORF66 polyclonal antiserum. Following three

5-min washes with PBS, the secondary antibodies, fluorescein isothiocyanate-coupled anti-mouse and Texas Red-coupled anti-rabbit (Jackson ImmunoResearch, Inc., West Grove, PA), were added for 45 min at 37°C and shielded from light. Coverslips were mounted with Vectashield containing 4′,6′-diamidino-2-phenylindole nuclear stain (Vector Laboratories, Inc., Burlingame, CA) and stored in the dark. Imaging was performed at the Cell Sciences Imaging Facility (Stanford, CA) with a Zeiss LSM 510 confocal laser scanning microscope (Carl Zeiss, Inc.).

Transmission electron microscopy. T-cell xenografts were recovered from SCID-hu mice at day 14 postinoculation and immediately fixed with 2% glutaraldehyde in 0.1 M phosphate buffer (PBS), pH 7.0, for 2 hours. The specimens were then washed twice in PBS and postfixed with 1% osmium tetroxide (Polysciences, Inc., Warrington, PA) in PBS for 1 hour. After two 10-minute washes in double distilled water, specimens were stained in 0.25% uranyl acetate (Polysciences, Inc.) overnight. After 24 h, the specimens were washed with water and dehydrated through a graded series of alcohol and propylene oxide washes. Each sample was infiltrated sequentially with 2:1 and 1:1 propylene oxide-EPON (Resolution Performance Products, Houston, TX) for 4 h, incubated overnight with 100% EPON, transferred to fresh EPON, and embedded and polymerized at 60°C for 24 h. Thin sections were collected on copper grids, stained with uranyl acetate and lead citrate, and viewed using a Phillips CM-12 transmission electron microscope.

Melanoma cells were infected with 1,000 CFU and grown on glass coverslips for 72 h. The cells were then fixed for 35 min and fixed/stained as described above. Cells were embedded by placing gelatin capsules filled with resin on top of the coverslip and spraying them with liquid nitrogen.

Flow cytometric detection of caspase 3 activation and intracellular phosphoprotein expression in T cells. Primary T cells were isolated from human tonsils obtained from the Department of Pathology at the Stanford University Medical Center according to a protocol approved by the Stanford University Committee for research involving human subjects. The tonsils were dissociated to single cells and prepared as previously described (28). An affinity T-cell column was used to separate out the T cells to more than 95% purity (Pierce, Inc.). T cells were cocultured with virus-infected HELF cell monolayers and harvested 48 h after infection. T cells were stained with FITC-conjugated monoclonal rabbit anti-active caspase 3 antibody according to the manufacturer's Apoptosis Kit 1 protocol (BD Biosciences, San Diego, CA). To identify VZV-infected tonsillar T cells, cells were stained with monoclonal antibodies specific for human CD3 (clone S4.1, conjugated to TRI-COLOR; Caltag) and VZV-immune or non-VZV-immune polyclonal human serum (IgG purified) along with Alexa Fluor 647-conjugated goat anti-human IgG (H+L; Molecular Probes, Eugene, OR).

For intracellular phosphoprotein flow cytometry experiments, T cells were stimulated with 10 ng/ml gamma interferon (Peprotech, Rocky Hill, NJ), 50 ng/ml phorbol myristate acetate (PMA; Sigma), and 1 μM ionomycin (CalBioChem, San Diego, CA) or 2 μg/ml anti-T-cell receptor (anti-TCR; clone OKT3) and 1 μg/ml anti-CD28 (clone 28.1), added directly to culture medium for 10 min. The T cells were transferred immediately to paraformaldehyde (1.5% final concentration), vortexed briefly, incubated at room temperature for 10 min, washed, stained with anti-VZV IgG and anti-human IgG-FITC as described above, washed again, and permeabilized in 90% methanol on ice for 30 min. The aliquots were stained with antibodies to CD3 (Cy5.5 conjugated) and phosphorylated proteins phospho-Stat1 (Stat91/84, clone 4a, Y701), phospho-ERK1/2 (clone 20a, pT202/pY204), and phopho-p38 MAPK (clone 36, pT180/pY182) conjugated to Alexa Fluor 647 (BD Biosciences).

RESULTS

Construction of pOka recombinants with ORF66 mutations. The ORF66 gene, which consists of a 1,181-bp sequence located in the unique short region of the VZV genome, was deleted from cosmid pvSpe23 (Fig. 1D). Since the complete deletion of ORF66 overlaps with promoter sequences (pOka nt 114,293 to 114,328; Dumas nt 113,037 to 114,225) important for expression of the adjacent ORF67 (gI), a second, partial deletion (pOka nt 113,140 to 114,273; Dumas nt 113,140 to 114,170) was also made that does not disrupt the ORF67 promoter region (17). Of interest, neither the complete nor the partial ORF66 deletion allowed viral replication; recombinant virus was not recovered in three of three transfections with five separately derived pvSpe23 mutant cosmids that had the complete ORF66 deletion or in three of three transfections with four independently generated cosmids with the partial deletion of ORF66. Although the partial ORF66 deletion could be rescued by insertion of ORF66 into the nonnative AvrII site, the complete deletion was not rescued in three of three experiments with four separately derived ΔORF66 cosmids. A stop codon insertion mutant, pOka66S (Fig. 1E), yielded infectious virus in three independent transfections.

In addition, two point mutants, pOka66S48A and pOka66S331A (Fig. 1F), were recovered when these serines in putative phosphorylation sites of ORF66 protein were changed to alanines. These two mutations were made in residues that were selected by NetPhos as sites in ORF66 that were very likely to be phosphorylated (7). The S48A mutation was made in the sequence ESEDD (amino acids 47 to 51), which is a consensus sequence for phosphorylation by ORF47, the other VZV kinase. This sequence has previously been identified to be S/T-x-D/E-D/E, in which the amino acids +1 and −1 are acidic (20). The S331A mutation was made in the KRSS sequence (amino acids 329 to 332) of ORF66, which could be a consensus sequence for phosphorylation by two cellular kinases that resemble ORF66: protein kinase A (cyclic AMP-dependent protein kinase), whose consensus phosphorylation site is R-R/K-x-S/T (19), and gamma-PAK (PAK2), whose consensus phosphorylation site is K/R-R-x-S/T (52).

Expected ORF66 sequences in recombinant mutant and rescued viruses were confirmed by sequencing full-length PCR products (data not shown). ORF66 protein was not detected by SDS-polyacrylamide gel electrophoresis and immunoblot analysis with ORF66-specific antibodies in lysate from cells infected with pOka66S (Fig. 1G) or in uninfected melanoma cells. However, it was clearly visible as a 48-kDa band in melanoma cells infected with pOka, pOka66S48A, and pOka66S331A. In other experiments, a myc tag was inserted within the ORF66 C terminus, upstream of the ORF67 promoter, and the ORF66 protein was detected using an anti-myc antibody in pOka-infected, but not in pOka66S-infected, melanoma cells by immunofluorescence (data not shown). This antibody also precipitated ORF66 protein from the lysate of MeWo cells infected with pOka, but not pOka66S, and did not reveal the presence of truncated ORF66 protein (data not shown).

Kinchington et al. previously demonstrated that the ORF66 protein is required for translocation of IE62, the major VZV gene transactivator, from the nucleus to the cytoplasm in later stages of infection (22, 23). Analysis of the localization of the IE62 and ORF66 proteins in melanoma cells by confocal microscopy at 72 h postinfection reveals that while IE62 localizes to both the nucleus and the cytoplasm of pOka-infected cells, it is strictly nuclear in the pOka66S-infected cells (data not shown). However, unlike pOka66S, the mutations of ORF66 residues S_{48} and $S_{331/332}$ in the pOka66S48A and pOka66S331A viruses do not restrict IE62 localization to the nucleus (data not shown).

Replication of pOka66S in vitro. The pOka66S virus displayed slightly reduced growth by infectious center assay in melanoma cells at days 3, 4, and 5, compared with pOka ($P = 0.004$, $P = 0.015$, and $P = 0.022$) (Fig. 2A). While pOka grew to approximately 3×10^5 infectious foci/ml, pOka66S remained below 1×10^5 infectious foci/ml. These results differed

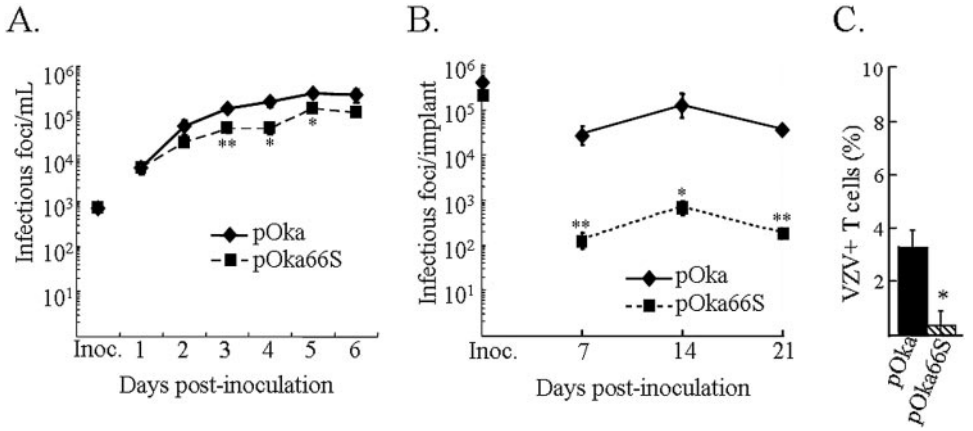

FIG. 2. Effects of pOka66S mutation on VZV growth in vitro and in T-cell xenografts in vivo. (A) Melanoma cells were inoculated on day zero with 1×10^3 CFU of pOka or pOkaORF66S. Two pOka66S mutant viruses were generated and tested independently. Aliquots were harvested daily for 6 days, and the number of infectious foci was determined by titration on melanoma cell monolayers. Each time point represents the mean of results for at least three wells. The *x* axis shows the days after inoculation when infected cell monolayers were harvested, and the *y* axis shows infectious foci per milliliter by infectious focus assay. One asterisk indicates that titers were significantly different from pOka ($P < 0.05$) at the same time point, while two asterisks indicate a difference with a *P* value of <0.01. (B) T-cell xenografts were inoculated with HEL fibroblasts infected with pOka or pOka66S on day zero (inoculum titers are shown on the *y* axis) and harvested weekly. T-cell suspensions were prepared, and titers were determined by infectious center assay. Each time point represents the mean number of plaques from two to four implants. Implants in which infectious virus was not recovered were excluded. One asterisk indicates that titers were significantly different from pOka with a *P* value of <0.05 at the same time point, while two asterisks indicate a difference with a *P* value of <0.001. (C) T cells from T-cell xenografts harvested at day 7 postinoculation with pOka or pOka66S were stained for expression of CD3 and VZV proteins and analyzed by flow cytometry. The bars indicate the percentage of VZV-positive T cells ± the standard error. One asterisk indicates a difference with a *P* value of <0.001.

from previous studies of the replication of ROKA66S, derived from vOka cosmids, which was equivalent to vOka in cultured melanoma cells (14, 37). However, the average plaque size for pOka66S (0.87 ± 0.13 mm) was not significantly different from pOka (0.90 ± 0.10 mm).

Replication of pOka66S in human T-cell xenografts. In order to assess the contribution of ORF66 to VZV virulence in T cells using pOka-derived mutants, T-cell xenografts were inoculated with pOka and pOka66S (Fig. 2B). The pOka virus titer by infectious center assay at day 7 ($>2 \times 10^4$ infectious foci/implant) was significantly higher than that of the pOka66S virus, which yielded only 1×10^2 infectious foci/implant at day 7 and peaked below 1×10^3 infectious foci/implant at day 14. pOka infection peaked with a titer of 1×10^5 infectious foci/implant at day 14. The growth differences between pOka and pOka66S were confirmed by immunohistochemistry (not shown) and by flow cytometric analysis of infected T cells from T-cell xenografts taken at 7 days postinoculation (37). The percentage of VZV-infected T cells from pOka-infected T-cell xenografts was approximately fivefold higher than the percentage from pOka66S-infected xenografts at this early time point (Fig. 2C). Previous histological evidence has shown that severe thymocyte depletion occurs in VZV-infected T-cell xenografts and that viral titers decrease at later stages of xenograft infection (35).

Virion formation in human T cells in SCID-hu T-cell xenografts infected with pOka or pOka66S in vivo. To further investigate VZV T-cell tropism and the 2-log reduction in growth of pOka66S in T cells, T-cell xenografts were removed at 14 days postinoculation with pOka or pOka66S and analyzed by transmission electron microscopy (TEM) (Fig. 3). Many complete nucleocapsids with a dark core (VZV genome) as well as empty capsids were visualized within the nuclei of T cells in xenografts infected with pOka (Fig. 3A). Significantly fewer nucleocapsids were observed in pOka66S-infected T cells (Fig. 3B). The average number of capsids per pOka-infected cell nucleus was 35 ± 13 ($n = 14$), while the average number of capsids per pOka66S-infected cell nucleus was only 3 ± 1 ($n = 3$; $P = 0.047$). One pOka66S-infected cell, shown in Fig. 3B, contained two complete nucleocapsids and several empty capsids in the nucleus. VZV nucleocapsids assemble in nuclei as icosahedral capsids enclosing the 125-kb VZV genome. The nucleocapsids and DNA cores in both pOka- and pOka66S-infected T cells appeared to be regular and intact. Both pOka and pOka66S nucleocapsids were present individually in the nucleoplasm, but only the much more abundant pOka nucleocapsids were clustered in the nucleus. The pOka-infected T cells contained spherical, membrane-defined intranuclear inclusions filled with complete nucleocapsids; nucleocapsids were also located immediately adjacent to these structures (Fig. 3C and D). In addition, virions at various stages of assembly and located at several intracellular sites were readily detected in the cytoplasm of pOka-infected T cells (Fig. 3E). Although significantly fewer virions could be found in pOka66S-infected T cells, those observed were morphologically comparable to pOka virions (Fig. 3F). The average number of virions in the cytoplasm of pOka-infected T cells was 10 ± 5 ($n = 14$), while the average number of virions in the cytoplasm of pOka66S-infected T cells was only 2 ± 1 ($n = 6$; $P = 0.047$). Importantly, in contrast to infected T cells, the number and intracellular location of virions were indistinguishable in melanoma cells infected with pOka and pOka66S in vitro (Fig. 4).

Further stages in VZV virion formation were also documented in T cells infected with pOka in vivo. Following assembly in the nucleus, complete nucleocapsids bud at the inner

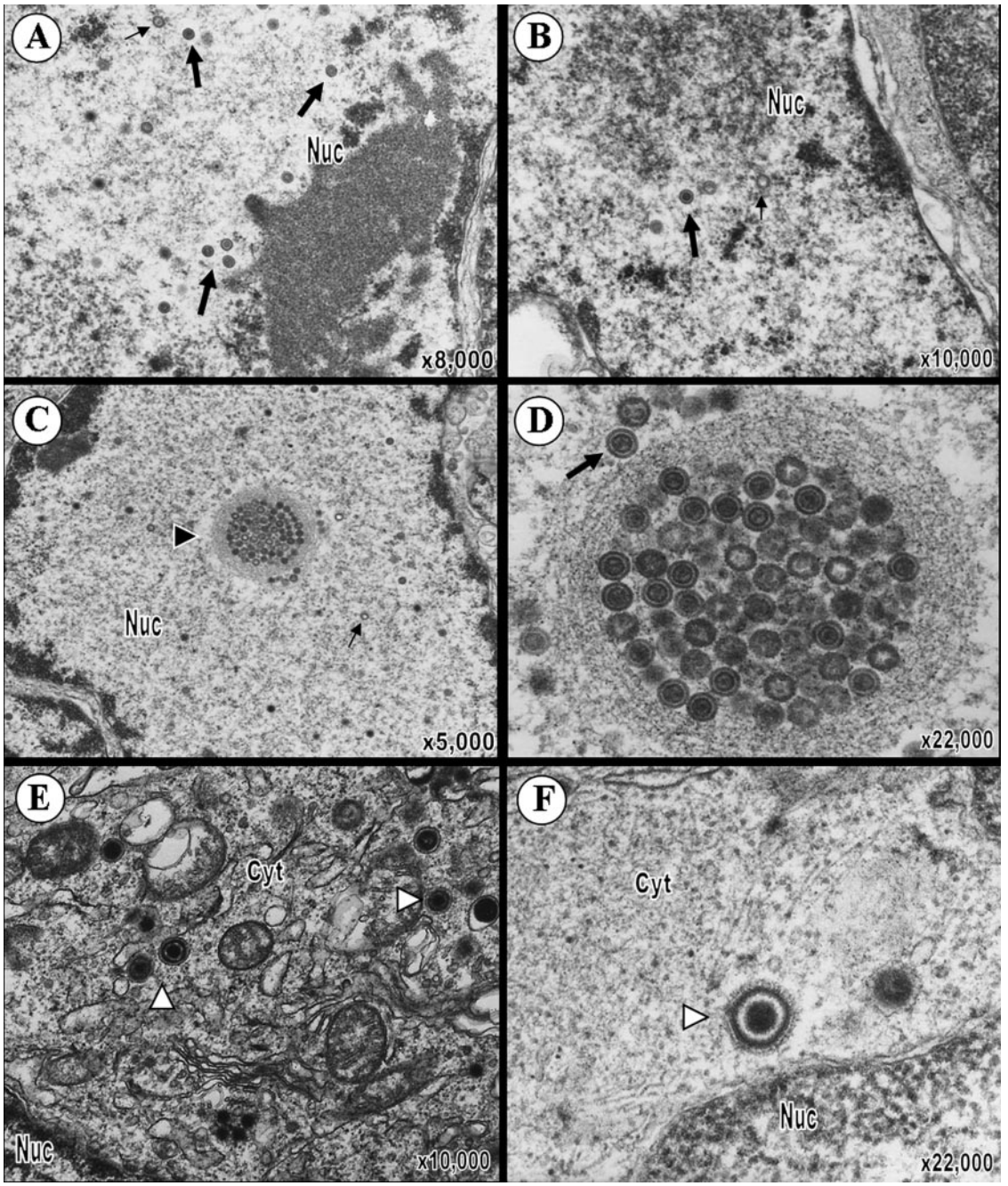

FIG. 3. VZV virion morphology in T cells infected with pOka or pOka66S. (A and B) At 14 days postinoculation, VZV nucleocapsids were present within the nuclei of T cells infected with pOka (A) or pOka66S (B). While most nucleocapsids contained a dark VZV DNA core (large arrows), some empty capsids were also seen (small arrows). (C) Virions were abundant in the nuclei of pOka-infected T cells and were present both individually and in clusters within the nucleoplasm. An arrowhead points to an example of an intranuclear vesicle containing virions in this pOka-infected cell. (D) Higher magnification of the intranuclear vesicle revealed the presence primarily of naked nucleocapsids containing the VZV pOka DNA core. (E and F) Complete virions (indicated by white arrowheads) were also found in the cytoplasm of cells infected with either pOka (E) or pOka66S (F). These viral particles were usually surrounded by vesicles and consisted of a complete capsid enclosed by viral tegument, envelope, and glycoprotein spikes. The magnification and locations of cytoplasm (cyt) and nucleus (nuc) are indicated.

leaflet of the nuclear membrane, through the perinuclear space, and into the cytoplasm. During herpesviral replication, mature nucleocapsids appear to undergo initial envelopment at the nuclear membrane, followed either by de-envelopment in the cytoplasm and secondary envelopment in the *trans*-Golgi network or by secondary envelopment without de-envelopment (6, 12, 33, 34, 46). A number of nucleocapsids budding through the nuclear membrane were observed in pOka-infected T cells (Fig. 5). Several nucleocapsids in various stages of egress were found in the nucleus adjacent to the inner

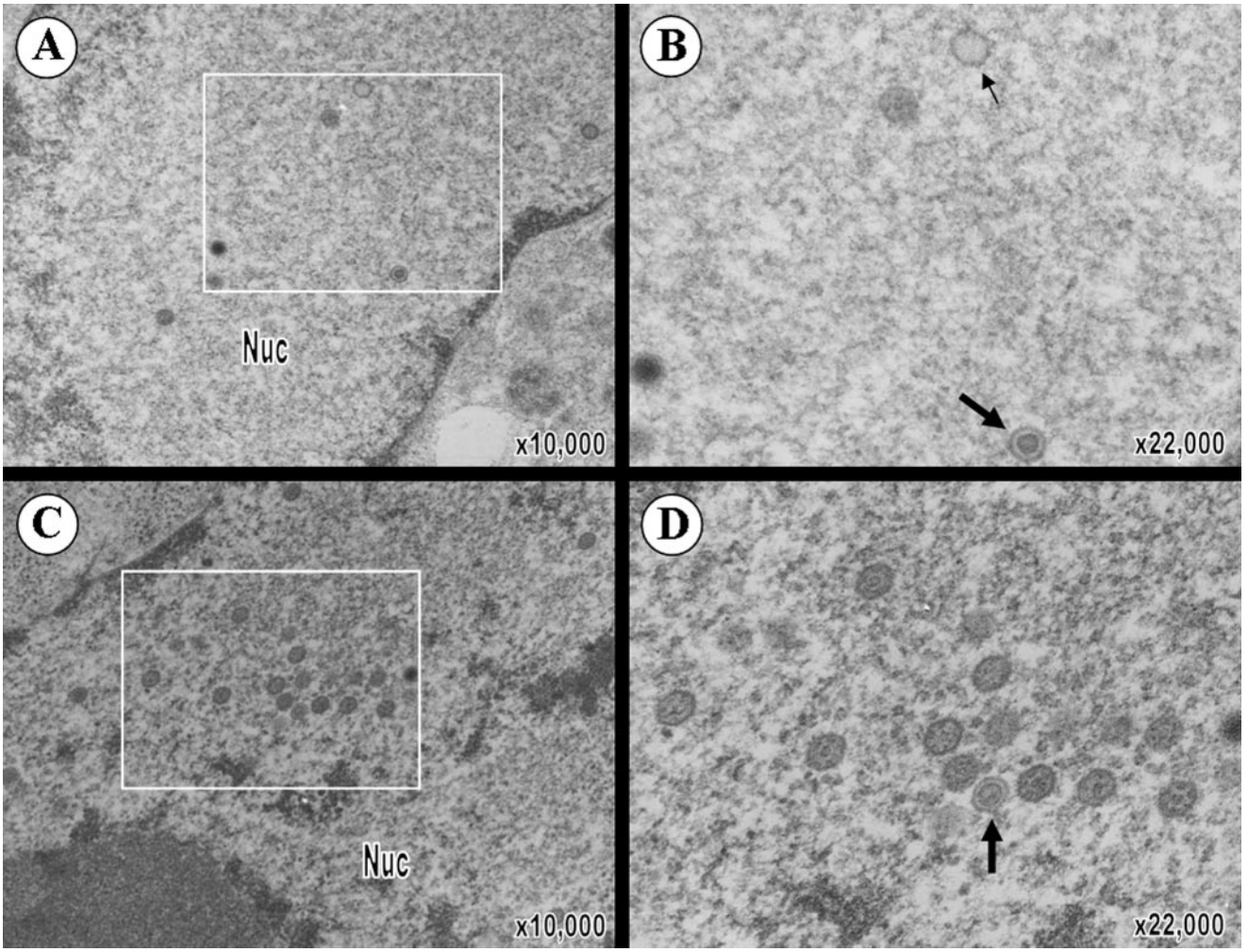

FIG. 4. VZV virion formation in melanoma cells in vitro. (A) Virions were clearly distinguishable in the nucleus of pOka-infected melanoma cells. (B) Magnification of pOka virions from the boxed area of panel A shows the presence of intranuclear virions (large arrows) and empty capsids (small arrows). (C) Virions were also abundantly present in the nucleus of pOka66S-infected melanoma cells. (D) Magnification of the boxed area of panel C shows that these nucleocapsids have a normal appearance comparable to those in pOka-infected cells. The magnification and locations of cytoplasm (cyt) and nucleus (nuc) are indicated.

nuclear membrane, causing alterations in this membrane ranging from a slight indentation (Fig. 5A) to nearly complete enclosure of the nucleocapsid (Fig. 5B). Virions were also observed in the perinuclear cleft (Fig. 5C) and were characterized by their increased size compared with capsids in the nucleus and by the addition of an envelope that appeared to have a smooth surface. Complete enveloped virions were found individually within vesicles in the cytosol of pOka-infected T cells (Fig. 5D). These cytoplasmic virions were larger than the budding nucleocapsids and typically had a central complete nucleocapsid surrounded by a uniform tegument, an intact viral envelope with clearly visible surface projections, and a single vesicle membrane. Very few tegumented, but nonenveloped, capsids were observed in the cytoplasm; however, one naked nucleocapsid was captured in the process of budding into a vesicle in the cytoplasm (Fig. 5E, inset). Final pOka virion egress through the plasma membrane was most easily observed in heavily infected T cells, where large vesicles appeared to release a number of virions simultaneously into the extracellular space (Fig. 5E and F).

Replication of pOka66S in human skin xenografts. The growth of the pOka virus in SCID-hu skin tissue at day 14 postinoculation was approximately 3×10^2 infectious foci/implant, and the titer declined at days 21 and 28 (Fig. 6). The pOka66S titer was significantly lower at day 14, with 7×10^1 infectious foci/implant ($P < 0.001$), and remained below 2×10^2 infectious foci/implant at all three times, although the absolute differences in pOka and pOka66S titers were minimal. Growth of the pOka66S virus peaked later, at day 21 postinoculation, with a titer of approximately 1×10^2 infectious foci/implant. The altered ORF66 sequence was confirmed for all mutants recovered from skin xenografts (data not shown).

Flow cytometric analysis of apoptosis in T cells. The ability of HSV-1 U_S3 to block apoptosis prompted the investigation of apoptosis in T cells infected with pOka or pOka66S in vitro. Active caspase 3 expression was used as a marker for induction

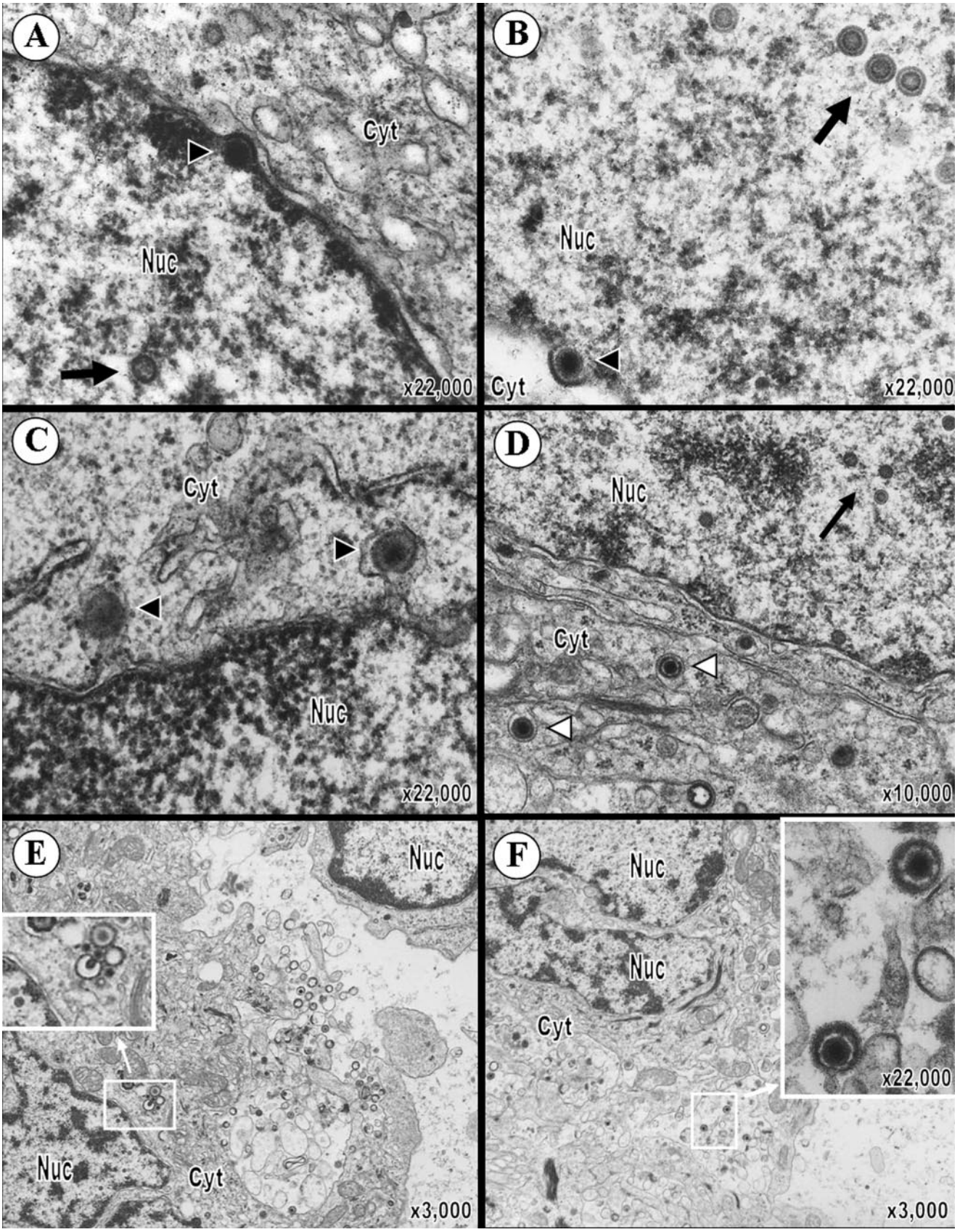

FIG. 5. Perinuclear and cytoplasmic localization of pOka virions within human T cells in SCID-hu T-cell xenografts. VZV nucleocapsids can be seen budding at the inner nuclear membrane (A and B). Arrowheads point to budding virions. In panel A, the indicated budding nucleocapsid

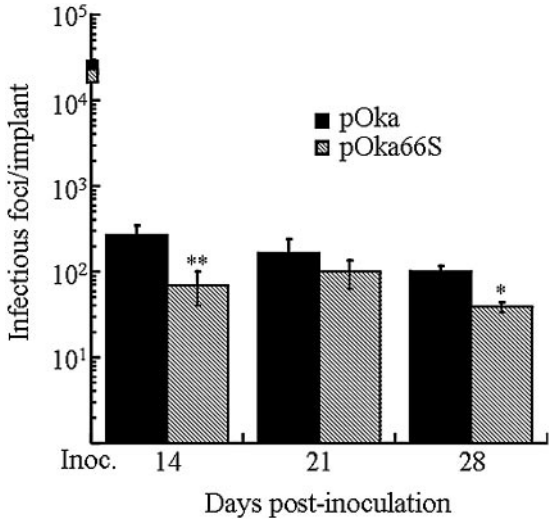

FIG. 6. Replication of VZV ORF66 mutants in skin xenografts in SCID-hu mice. Skin tissue was infected with pOka and pOka66S grown in HEL fibroblasts. Implants were harvested after 14, 21, and 28 days, and virus was titrated on melanoma cell monolayers by infectious focus assay. Each time point represents the mean number of plaques from three to four implants. Implants that did not contain infectious virus were excluded from the average. Inocula (shown as boxes on the *y* axis) are given as infectious foci/100 μl, which represents the amount used to infect each implant. One asterisk indicates that titers were significantly different from pOka with a P value of <0.01 at the same time point, while two asterisks indicate a difference with a P value of <0.001.

of the apoptotic pathway. After 48 h of coculture with either pOka- or pOka66S-infected fibroblasts, T cells were stained for VZV proteins, CD3, and active caspase 3. The populations were then gated on CD3-positive T cells (Fig. 7A; left panels show gating). The percentage of total T cells that expressed active caspase 3 was more than fivefold higher in pOka66S-infected cultures than in pOka-infected cultures (Fig. 7A, right panels). When T cells were further gated on the VZV-positive population, greater than 23% of the $CD3^+$, VZV^+ pOka66S-infected T cells were found to express activated caspase 3, compared with less than 2.6% of $CD3^+$, VZV^+ T cells infected with pOka (Fig. 7B, top panel). In both cultures, less than 1.7% of the VZV-negative T-cell population was undergoing apoptosis based on active caspase 3 expression (Fig. 7B, bottom panel). Infection of melanoma or fibroblast cells showed no difference in active caspase 3 expression between pOka- and pOka66S-infected cells at 24, 48, or 72 h postinfection (data not shown).

Flow cytometric analysis of phospho-protein expression. The regulation of a number of protective and proliferative signals within cells requires the phosphorylation of intracellular signaling proteins. Based on the hypothesis that reduction in VZV growth in T cells, but not melanoma cells, in the absence of the ORF66 kinase may be due to differences in target cell signaling, we explored whether VZV infection altered cellular signaling in response to external stimuli, and whether such effects might be due to ORF66 kinase activity. Phospho-protein flow cytometric analysis was used to reveal differences in the phosphorylation state of three intracellular signaling proteins, Stat1, Erk1/2, and p38, in infected and uninfected T cells (16, 25, 26). Human tonsil T cells that were uninfected or infected for 48 or 72 h with either pOka or pOka66S were stimulated with recombinant human IFN-γ, PMA, and ionomycin, or anti-TCR and anti-CD28, for 10 minutes at 37°C, and alterations in the phosphorylation state of these three important proteins were determined by staining with phospho-specific antibodies followed by flow cytometry. In the analysis, T cells were gated to definitively separate the VZV-positive and VZV-negative cells. An intermediate population was observed in these experiments with VZV fluorescence intensity between 10^1 and 10^2 on the *x* axis, which is distinctly negative for Stat1 phosphorylation following IFN-γ treatment specifically in pOka-infected cells. To exclude this intermediate population from the analysis, the cutoff for VZV-negative T cells was placed at 10^1 on the *x* axis. By comparing cells with equivalent intensity of VZV protein staining, this analysis focuses on the most highly VZV-positive cells from each population and mitigates the effects of any delay in infection of pOka66S-infected T cells.

As expected, IFN-γ increased the percentage of mock-infected T cells with detectable phosphorylated Stat1 (pStat1) 60-fold (Fig. 8A and B, left panels). The mean pStat1 fluorescence intensity increased an average of 2.5-fold following IFN-γ treatment of mock-infected T cells in two independent experiments (Fig. 8C). However, induction of the IFN pathway, as assessed by Stat1 phosphorylation, was inhibited in pOka-infected tonsil T cells stimulated with IFN-γ. In the experiment shown, 11% of pOka-infected T cells expressed pStat1 after IFN-γ stimulation at 48 h postinfection (Fig. 8A and B, middle panels). In four experiments, pOka-infected cells at 48 h postinfection exhibited greater than twofold lower mean pStat1 fluorescence after IFN-γ treatment than uninfected cells from the same preparation ($P = 0.01$) (Fig. 8C). The effect on Stat1 phosphorylation was lower at 72 h in pOka-infected T cells, but it remained statistically significant ($P = 0.02$). Although pOka-infected T cells did not phosphorylate Stat1 in response to IFN-γ to the same extent as uninfected cells, this effect was not observed in pOka66S-infected cells at either 48 or 72 h postinfection. At 48 h postinfection, the pOka66S-infected cells retained an increase in mean

is adjacent to the inner leaflet of the nuclear membrane and the site of budding is marked by an area of increased electron density. In panel B, the budding viral particle is nearly completely surrounded by nuclear membrane. (C) Virions in the perinuclear cleft (indicated by black arrowheads) appear to have a tegument and envelope. (D) Complete enveloped virions can be seen within vesicles in the cytosol (white arrowheads) and are significantly larger than capsids in the nucleus (large arrows). (E) The inset shows the magnification of a nucleocapsid in the cytoplasm budding into a cytoplasmic vesicle. Next to this is a complete virion, an empty vesicle, three capsids containing a DNA core, and an empty capsid. Virions in various stages of maturation can be seen throughout the cell, as well as exiting the plasma membrane from a cytoplasmic vesicle. (F) Complete virions within a large cytoplasmic vesicle consist of a viral DNA core, capsid, tegument, envelope, and protein spikes (inset). The magnification and locations of cytoplasm (cyt) and nucleus (nuc) are indicated.

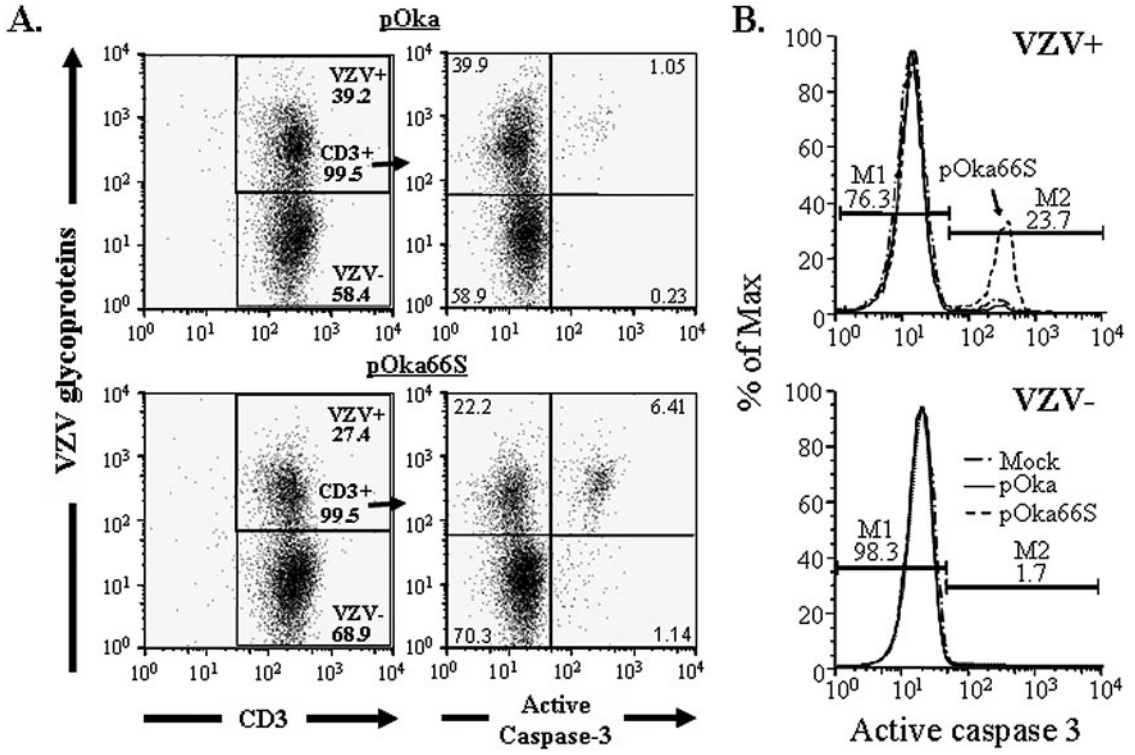

FIG. 7. Flow cytometric analysis of apoptosis in pOka- and pOka66S-infected T cells. Purified human tonsil T cells were infected with either pOka or pOka66S and stained at 48 h postinfection for VZV proteins, CD3, and active caspase 3. (A) Cells cultured with pOka-infected fibroblasts (top panels) or pOka66S-infected fibroblasts (bottom panels) were gated on CD3-positive T cells (gating shown in left panels). Only 1% of all T cells cocultured with pOka-infected cells expressed active caspase 3 (top right panel), compared with more than 6% of T cells cocultured with pOka66S (bottom right panel). (B) T cells were divided into VZV-positive (top panel) and VZV-negative (bottom panel) populations. Over 20% of the T cells infected with pOka66S had detectable active caspase 3 (top panel), whereas uninfected T cells from the same culture were almost entirely negative for the presence of active caspase 3 (bottom panel), as were those infected with pOka (top panel).

pStat1 fluorescence greater than twofold in response to IFN-γ treatment. Additionally, treatment of these T cells with PMA-ionomycin or anti-TCR plus anti-CD28 did not alter phosphorylation of Stat1 (data not shown). Evaluation of phospho-Erk1/2 and phospho-p38 showed no significant differences between the phosphorylation of uninfected, pOka-infected, or pOka66S-infected T cells following stimulation (data not shown). Thus, during the initial 72 h of T-cell infection, there is a measurable difference in phosphorylation of Stat1 in response to IFN-γ between pOka- and pOka66S-infected cells.

DISCUSSION

Investigations in the SCID-hu mouse model of VZV pathogenesis support the concept that primary VZV infection involves entry of infected T cells into the circulation during an initial viremic phase and that these migrating T cells carry infectious virus from sites of respiratory mucosal inoculation to the skin. Tonsil $CD4^+$ T cells, especially activated, memory subpopulations that are programmed for tissue immune surveillance, are highly permissive for VZV infection in vitro and can transfer virus from the circulation to human skin xenografts in the SCID-hu mouse model (28, 29). VZV must then overcome innate immune barriers, mediated by epidermal cell production of IFN-α, in order to create the characteristic vesicular cutaneous lesions (27, 29). In the current experiments, we have characterized the pattern of VZV virion formation within T cells in vivo and, using comparisons of pOka and pOka66S, a pOka-derived ORF66 stop codon mutant, we have identified the importance of the ORF66 protein for VZV virion production, interference with apoptosis, and inhibition of the IFN pathway in VZV-infected T cells.

Like all herpesviruses, VZV virion production must begin with the packaging of viral DNA in precursor procapsids in the nucleus of the infected cell (46). Our EM experiments showed that formation of VZV nucleocapsids and complete VZV virions was extensive in primary differentiated human T cells infected with pOka in vivo. Our EM analyses of skin xenografts have also shown production of authentic VZV virions in vivo, in contrast to the predominance of aberrant virions in cultured cells (6, 36). These observations are consistent with a role for release of intact VZV virions from T cells into skin during VZV pathogenesis and support our evidence that VZV must be released from T cells in order to infect other T cells in vivo (6).

Some pOka-infected T cells also had striking intranuclear inclusions with multiple membranous layers surrounding dense collections of capsids, which were not observed in epidermal cells. Similar membrane-bound nuclear structures have been found in T cells infected in vitro with human herpesvirus 6, which is a T-lymphotropic betaherpesvirus (45). The human

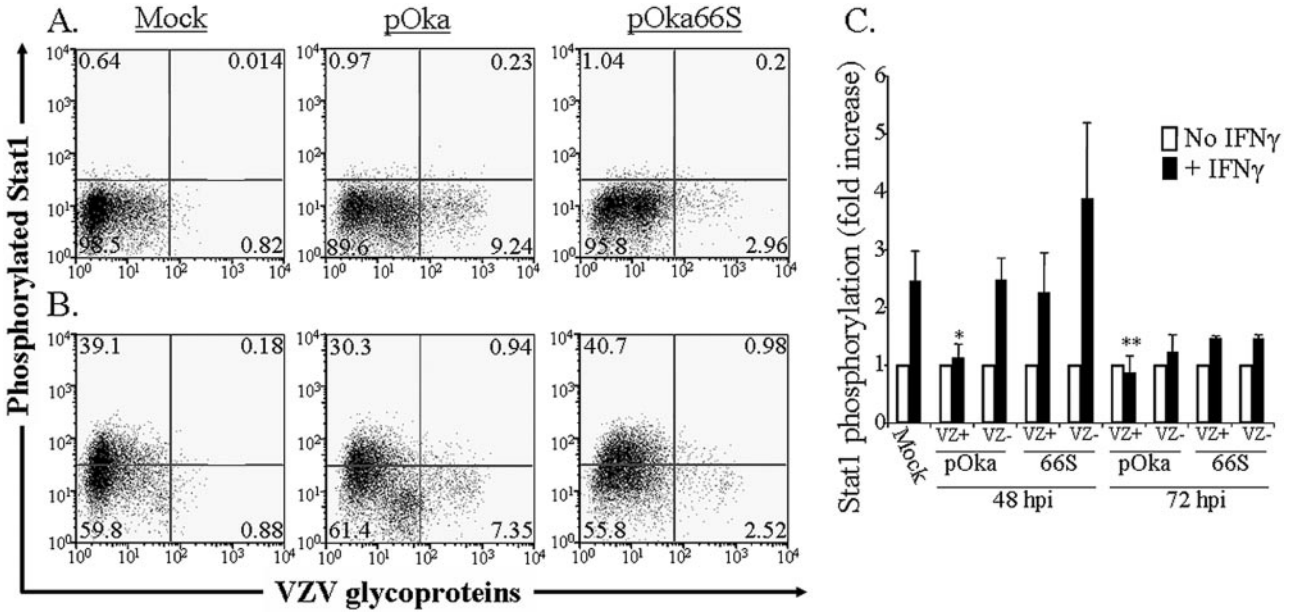

FIG. 8. Flow cytometric analysis of Stat1 phosphorylation in human tonsil T cells stimulated with IFN-γ. Column-purified human tonsil T cells were cocultured with VZV-infected HEL monolayers. After 48 h, cells were removed from the monolayer and either left unstimulated (A) or stimulated with recombinant human IFN-γ for 10 min at 37°C (B). Cells were fixed in paraformaldehyde, stained with antibodies and fluorescent conjugates to VZV proteins, permeabilized in methanol, and then stained with antibodies to phospho-Stat1 and CD3. FACS plots show anti-phospho-Stat1 versus anti-VZV staining of uninfected (left plots), pOka-infected (middle plots), and pOka66S-infected (right plots) tonsil T cells (gated on $CD3^+$ cells) without stimulation (A) or following stimulation with IFN-γ (B). (C) Data from T cells cultured for 48 or 72 h with infected HEL monolayers are shown as the average fold increase in phospho-Stat1 fluorescence intensity following IFN-γ treatment in VZV-infected and uninfected T cells for four independent experiments done after 48 h and two experiments combined for 72 h. One asterisk indicates a fold increase that is significantly different from that of uninfected cells from the same culture with $P = 0.01$, while two asterisks indicate a difference with $P = 0.02$.

herpesvirus 6 inclusions were termed "tegusomes" because the presence of partially tegumented capsids suggested that tegument acquisition might occur at these sites. However, pOka intranuclear virions did not appear to be tegumented, and many pOka-infected T cells contained virions without evidence of these structures, indicating that formation of intranuclear vesicles is not required for VZV nucleocapsid assembly in T cells infected within the intact tissue microenvironment in vivo.

Preventing ORF66 translation was associated with a dramatic reduction in VZV virulence in T-cell xenografts. The results with pOka66S were comparable to those obtained with vOka-derived ROKA66S, indicating that ORF66 protein is a critical determinant of infection of T cells by a low-passage clinical isolate as well as a tissue culture-passaged VZV strain (37). EM experiments showed that the difference between pOka and pOka66S replication reflected a marked decrease in the intranuclear assembly of nucleocapsids in pOka66S-infected T cells. These observations indicate that ORF66 protein is required for early events in VZV replication in T cells in vivo, in addition to its role in the nuclear exclusion of IE62 late in infection (23). The impact of preventing ORF66 translation on virion production was specific for T cells infected in vivo and was not observed in melanoma cells infected with pOka66S in vitro. When the ORF66 homologue U_S3 was deleted from pseudorabies virus, virions accumulated in the perinuclear space, suggesting a defect in de-envelopment (24, 44). This phenomenon was not observed in T cells infected with pOka66S, indicating that the ORF66 protein was not required for nuclear egress of VZV virions, to the extent that virions were made in the absence of the ORF66 protein. This difference may be due to the absence of a corresponding phosphorylation site for ORF66 kinase in the VZV homologue of U_L34, a target of HSV U_S3 (24, 43), or because ORF66 protein is not an absolutely essential structural component in primary VZV virions.

VZV spread in skin, as well as in cultured cells, is characterized by the formation of polykaryocytes and extensive syncytia resulting from cell-cell fusion. Syncytium formation can occur even when virion assembly is severely disrupted, as shown in studies of rOka47ΔC and rOka47D-N, two VZV mutants defective in ORF47 protein kinase activity (6, 35). In contrast, virion assembly and release of infectious virus particles appears to be necessary for T-cell tropism, because VZV-infected T cells do not undergo fusion with adjacent cells. The defective virion assembly of rOka47ΔC and rOka47D-N mutants was associated with a complete block in replication in T cells in vivo (6). Some VZV virion production was observed in T cells infected with pOka66S in vivo, consistent with detectable, albeit limited viral replication. Although ORF47 protein is a major VZV kinase/tegument protein, the analyses of pOka66S and vOka-derived ROKA66S demonstrate that ORF47 protein does not compensate for the absence of ORF66 protein functions in T cells. The deficiency in T-cell tropism associated with eliminating ORF66 protein appears to result from a defect in virion production specific for these target cells. In contrast to the ORF47 mutants, virion assembly

was not disrupted in pOka66S-infected melanoma cells and pOka66S infection was decreased only slightly in skin xenografts. This phenotype was not detected with ROka66S, probably because vOka is already attenuated for growth in skin (37). Thus, ORF66 protein appeared to provide a minor growth advantage in skin, perhaps because ORF47 protein function is sufficient or because an epidermal cell protein, not present in T cells, compensates for the lack of ORF66 protein.

If T-cell infection mediates VZV transfer from respiratory sites of inoculation to skin, modifying the induction of apoptosis in T cells may be useful during VZV pathogenesis. We found that T cells infected with pOka were protected from activation of caspase 3, a marker of apoptosis, compared to T cells infected with pOka66S. These data suggest that ORF66 protein may function to inhibit apoptosis in VZV-infected T cells. A number of studies have shown that deletion of HSV-1 U_S3, the ORF66 homologue, results in apoptosis of HSV-infected cells (10, 51). U_S3 has also been shown to prevent the cleavage activation of procaspase 3 and resulting caspase cascade in response to stress-inducing stimuli, likely through a mechanism involving interactions with Bcl-2 family proteins (4, 5, 8–11, 39, 40, 42). Previous observations about HSV-1 U_S3, combined with our new information about the effect of ORF66 on apoptosis in T cells, suggest that U_S3-related gene products such as the ORF66 protein interfere with apoptosis. Additionally, microarray analysis of the transcriptional profiles of VZV-infected primary human T cells and fibroblasts showed that the transcription of caspase 8 was decreased in infected T cells but not in HFFs or skin (18). Other evidence that may signify a tissue-specific antiapoptosis mechanism comes from the discovery by Hood et al. that VZV-infected human sensory neurons are resistant to apoptosis while HFFs are not (15).

Like other herpesviruses, VZV has evolved mechanisms for the transient evasion of host control by innate and adaptive immune mechanisms. Previous experiments showed that ORF66 contributes to the down-regulation of MHC class I cell surface expression on VZV-infected T cells (1). Our current experiments indicate that ORF66 protein may also help the virus to survive in infected T cells by inhibiting the signaling of the IFN pathway by IFN-γ. Such a mechanism could be important for VZV pathogenesis, since IFN-γ production by natural killer cells is an important innate immune response. VZV infection of fibroblasts inhibits IFN-γ signal transduction via the Jak/Stat pathway by causing a 10-fold reduction in Stat1α and a 90-fold reduction in Jak2 and an associated block in transcription of IFN regulatory factor 1 and class II transactivator in fibroblasts (2). IFN-γ-induced phosphorylation of Stat1 was reduced in pOka-infected T cells, but not in T cells infected with pOka66S. Thus, ORF66 protein may function to modulate the effects of IFN-γ on VZV infection of T cells as well as contributing to MHC class I down-regulation (1).

Although preventing ORF66 translation by inserting a stop codon into the pOka ORF66 gene was compatible with replication, as it was in vOka, these mutagenesis experiments demonstrated that complete or partial deletions of ORF66 did not allow recovery of infectious virus in our cosmid system. The observations with the complete deletion of ORF66, which overlaps with the gI (ORF67) promoter region, were consistent with our analyses of the gI (ORF67) promoter in the context of the VZV genome (17). The VZV gI protein is dispensable in vitro (30). Nevertheless, altering one of the ORF29 response elements of the gI promoter, designated 29RE4, did not allow VZV replication (13, 17). Of interest, neither the complete ORF66 deletion nor the 29RE4 substitution could be rescued, whereas the partial deletion of ORF66, which did not disrupt the 29RE4 region, was rescued by inserting the complete ORF66 sequence at the AvrII cloning site. These observations suggest that this region of the VZV genome has functions that are independent of expression of the ORF66 or gI proteins. In contrast, conservative substitutions in putative phosphorylation sites of the ORF66 protein at residues 48 and 331 had no effect on pOka replication in vitro or in T cells or skin in vivo.

In summary, VZV infection of T cells was associated with robust virion production and modulation of the apoptosis and IFN pathways in human T cells. Preventing ORF66 protein expression impaired the growth of the low-passage pOka virus in SCID-hu T-cell xenografts in vivo, increased the susceptibility of infected T cells to apoptosis, and reduced the capacity of the virus to interfere with induction of the interferon pathway by exposure to IFN-γ. Our working model is that VZV pathogenesis depends on the assembly and release of virions from T cells and that infected T cells must survive long enough to transport VZV from respiratory sites of inoculation to the skin (27). ORF66 protein appears to have a unique role in virion production that is specific for T cells and also supports VZV T-cell tropism by contributing to immune evasion and enhancing survival of infected T cells.

ACKNOWLEDGMENTS

This work was supported by grants AI053846 and AI20459 (A.M.A.) from the National Institute of Allergy and Infectious Diseases and a Stanford Graduate Fellowship from the Susan P. Markey Foundation (A.S.).

We thank Nafisa Ghori for assistance with transmission electron microscopy and Matthew Hale for helpful discussion regarding phospho-antibody flow cytometry techniques. SCID-hu (thy/liv) mice were kindly provided by Cheryl Stoddard (Gladstone Institute, University of California, San Francisco).

REFERENCES

1. **Abendroth, A., I. Lin, B. Slobedman, H. Ploegh, and A. M. Arvin.** 2001. Varicella-zoster virus retains major histocompatibility complex class I proteins in the Golgi compartment of infected cells. J. Virol. **75:**4878–4888.
2. **Abendroth, A., B. Slobedman, E. Lee, E. Mellins, M. Wallace, and A. M. Arvin.** 2000. Modulation of major histocompatibility class II protein expression by varicella-zoster virus. J. Virol. **74:**1900–1907.
3. **Arvin, A.** 2001. Varicella-zoster virus, p. 2731–2767. *In* D. M. Knipe and P. M. Howley (ed.), Fields virology. Lippincott Williams & Wilkins, Philadelphia, Pa.
4. **Aubert, M., and J. A. Blaho.** 2001. Modulation of apoptosis during herpes simplex virus infection in human cells. Microbes Infect. **3:**859–866.
5. **Benetti, L., J. Munger, and B. Roizman.** 2003. The herpes simplex virus 1 US3 protein kinase blocks caspase-dependent double cleavage and activation of the proapoptotic protein BAD. J. Virol. **77:**6567–6573.
6. **Besser, J., M. Ikoma, K. Fabel, M. H. Sommer, L. Zerboni, C. Grose, and A. M. Arvin.** 2004. Differential requirement for cell fusion and virion formation in the pathogenesis of varicella-zoster virus infection in skin and T cells. J. Virol. **78:**13293–13305.
7. **Blom, N., S. Gammeltoft, and S. Brunak.** 1999. Sequence- and structure-based prediction of eukaryotic protein phosphorylation sites. J. Mol. Biol. **294:**1351–1362.
8. **Chao, D. T., and S. J. Korsmeyer.** 1998. Bcl-2 family: regulators of cell death. Annu. Rev. Immunol. **16:**395–419.
9. **Galvan, V., R. Branimarti, J. Munger, and B. Roizman.** 2000. Bcl-2 blocks a caspase-dependent pathway of apoptosis activated by herpes simplex virus 1 infection in HEp-2 cells. J. Virol. **74:**1931–1938.
10. **Galvan, V., R. Branimarti, and B. Roizman.** 1999. Herpes simplex virus 1 blocks caspase-3-independent and caspase-dependent pathways to cell death. J. Virol. **73:**3219–3226.

11. **Galvan, V., and B. Roizman.** 1998. Herpes simplex virus 1 induces and blocks apoptosis at multiple steps during infection and protects cells from exogenous inducers in a cell-type-dependent manner. Proc. Natl. Acad. Sci. USA **95:**3931–3936.
12. **Granzow, H., B. G. Klupp, W. Fuchs, J. Veits, N. Osterrieder, and T. C. Mettenleiter.** 2001. Egress of alphaherpesviruses: comparative ultrastructural study. J. Virol. **75:**3675–3684.
13. **He, H., D. Boucaud, J. Hay, and W. T. Ruyechan.** 2001. *cis* and *trans* elements regulating expression of the varicella zoster virus gI gene. Arch. Virol. Suppl. **17:**57–70.
14. **Heineman, T. C., K. E. Seidel, and J. I. Cohen.** 1996. The varicella-zoster virus ORF66 protein induces kinase activity and is dispensable for viral replication. J. Virol. **10:**7312–7317.
15. **Hood, C., A. L. Cunningham, B. Slobedman, R. A. Boadle, and A. Abendroth.** 2003. Varicella-zoster virus-infected human sensory neurons are resistant to apoptosis, yet human foreskin fibroblasts are susceptible: evidence for a cell-type-specific apoptotic response. J. Virol. **77:**12852–12864.
16. **Irish, J. M., R. Hovland, P. O. Krutzik, O. D. Perez, O. Bruserud, B. T. Gjertsen, and G. P. Nolan.** 2004. Single cell profiling of potentiated phospho-protein networks in cancer cells. Cell **118:**217–228.
17. **Ito, H., M. H. Sommer, L. Zerboni, H. He, D. Boucaud, J. Hay, W. Ruyechan, and A. M. Arvin.** 2003. Promoter sequences of varicella-zoster virus glycoprotein I targeted by cellular transactivating factors Sp1 and USF determine virulence in skin and T cells in SCIDhu mice in vivo. J. Virol. **77:**489–498.
18. **Jones, J. O., and A. M. Arvin.** 2003. Microarray analysis of host cell gene transcription in response to varicella-zoster virus infection of human T cells and fibroblasts in vitro and SCIDhu skin xenografts in vivo. J. Virol. **77:** 1268–1280.
19. **Kennelly, P. J., and E. G. Krebs.** 1991. Consensus sequences as substrate specificity determinants for protein kinases and protein phosphatases. J. Biol. Chem. **266:**15555–15558.
20. **Kenyon, T. K., E. Homan, J. Storlie, M. Ikoma, and C. Grose.** 2003. Comparison of varicella-zoster virus ORF47 protein kinase and casein kinase II and their substrates. J. Med. Virol. **70:**S95–S102.
21. **Kenyon, T. K., J. Lynch, J. Hay, W. Ruyechan, and C. Grose.** 2001. Varicella-zoster virus ORF47 protein serine kinase: characterization of a cloned, biologically active phosphotransferase and two viral substrates, ORF62 and ORF63. J. Virol. **75:**8854–8858.
22. **Kinchington, P. R., K. Fite, A. Seman, and S. E. Turse.** 2001. Virion association of IE62, the varicella-zoster virus (VZV) major transcriptional regulatory protein, requires expression of the VZV open reading frame 66 protein kinase. J. Virol. **75:**9106–9113.
23. **Kinchington, P. R., K. Fite, and S. E. Turse.** 2000. Nuclear accumulation of IE62, the varicella-zoster virus (VZV) major transcriptional regulatory protein, is inhibited by phosphorylation mediated by the VZV open reading frame 66 protein kinase. J. Virol. **74:**2265–2277.
24. **Klupp, B. G., H. Granzow, and T. C. Mettenleiter.** 2001. Effect of the pseudorabies virus US3 protein on nuclear membrane localization of the UL34 protein and virus egress from the nucleus. J. Gen. Virol. **82:**2363–2371.
25. **Krutzik, P. O., J. Irish, G. P. Nolan, and O. D. Perez.** 2004. Analysis of phospho-proteins by flow cytometry: techniques and clinical applications. Clin. Immunol. **110:**206–221.
26. **Krutzik, P. O., and G. P. Nolan.** 2003. Intracellular phospho-protein staining techniques for flow cytometry: monitoring single cell signaling events. Cytometry **55A:**61–70.
27. **Ku, C. C., J. Besser, A. Abendroth, C. Grose, and A. M. Arvin.** 2005. Varicella-zoster virus pathogenesis and immunobiology: new concepts emerging from investigations with the SCIDhu mouse model. J. Virol. **79:** 2651–2658.
28. **Ku, C. C., J. A. Padilla, C. Grose, E. C. Butcher, and A. M. Arvin.** 2002. Tropism of varicella-zoster virus for human tonsillar $CD4^+$ T lymphocytes that express activation, memory, and skin homing markers. J. Virol. **76:** 11425–11433.
29. **Ku, C. C., L. Zerboni, H. Ito, B. S. Graham, M. Wallace, and A. M. Arvin.** 2004. Varicella-zoster virus transfer to skin by T cells and modulation of viral replication by epidermal cell interferon-alpha. J. Exp. Med. **200:**917–925.
30. **Mallory, S., M. Sommer, and A. M. Arvin.** 1998. Analysis of the glycoproteins I and E of varicella-zoster virus (VZV) using deletional mutations of VZV cosmids. J. Infect. Dis. **178**(Suppl. 1)**:**S22–S26.
31. **Mallory, S., M. Sommer, and A. M. Arvin.** 1997. Mutational analysis of the role of glycoprotein I in varicella-zoster virus replication and its effects on glycoprotein E conformation and trafficking. J. Virol. **71:**8279–8288.
32. **Meier, J. L., and S. E. Strause.** 1995. Interactions between varicella-zoster virus IE62 and cellular transcription factor USF in the coordinate activation of genes 28 and 29. Neurology **45:**S30–S32.
33. **Mettenleiter, T. C.** 2004. Budding events in herpesvirus morphogenesis. Virus Res. **106:**167–180.
34. **Mettenleiter, T. C.** 2002. Herpesvirus assembly and egress. J. Virol. **76:**1537–1547.
35. **Moffat, J. F., M. D. Stein, H. Kaneshima, and A. M. Arvin.** 1995. Tropism of varicella-zoster virus for human $CD4^+$ and $CD8^+$ T lymphocytes and epidermal cells in SCID-hu mice. J. Virol. **69:**5236–5242.
36. **Moffat, J. F., L. Zerboni, P. R. Kinchington, C. Grose, H. Kaneshima, and A. M. Arvin.** 1998. Attenuation of the vaccine Oka strain of varicella-zoster virus and role of glycoprotein C in alphaherpesvirus virulence demonstrated in the SCID-hu mouse. J. Virol. **72:**965–974.
37. **Moffat, J. F., L. Zerboni, M. H. Sommer, T. C. Heineman, J. I. Cohen, H. Kaneshima, and A. M. Arvin.** 1998. The ORF47 and ORF66 putative protein kinases of varicella-zoster virus determine tropism for human T cells and skin in the SCID-hu mouse. Proc. Natl. Acad. Sci. USA **95:**11969–11974.
38. **Montini, E., G. Andolfi, A. Caruso, G. Buchner, S. M. Walpole, M. Mariani, G. Consalex, D. Trump, A. Ballabio, and B. Franco.** 1998. Identification and characterization of a novel serine-threonine kinase gene from the Xp22 region. Genomics **51:**427–433.
39. **Munger, J., A. V. Chee, and B. Roizman.** 2001. The US3 protein kinase blocks apoptosis induced by the d120 mutant of herpes simplex virus 1 at a premitochondrial stage. J. Virol. **75:**5491–5497.
40. **Munger, J., and B. Roizman.** 2001. The US3 protein kinase of herpes simplex virus 1 mediates the posttranslational modification of BAD and prevents BAD-induced programmed cell death in the absence of other viral proteins. Proc. Natl. Acad. Sci. USA **98:**10410–10415.
41. **Niizuma, T., L. Zerboni, M. Sommer, H. Ito, S. Hinchliffe, and A. M. Arvin.** 2003. Construction of varicella-zoster virus recombinants from parent Oka cosmids and demonstration that ORF65 protein is dispensable for infection of human skin and T cells in the SCID-hu mouse model. J. Virol. **77:**6062–6065.
42. **Ogg, P. D., P. J. McDonell, B. J. Ryckman, C. M. Knudson, and R. J. Roller.** 2004. The HSV-1 Us3 protein kinase is sufficient to block apoptosis induced by overexpression of a variety of Bcl-2 family members. Virology **319:**212–224.
43. **Purves, F. C., D. Spector, and B. Roizman.** 1991. The herpes simplex virus 1 protein kinase encoded by the US3 gene mediates posttranslational modification of the phosphoprotein encoded by the UL34 gene. J. Virol. **65:**5757–5764.
44. **Reynolds, A., E. G. Wills, R. J. Roller, B. J. Ryckman, and J. D. Baines.** 2002. Ultrastructural localization of the herpes simplex virus type 1 UL31, UL34, and US3 proteins suggests specific roles in primary envelopment and egress of nucleocapsids. J. Virol. **76:**8939–8952.
45. **Roffman, E., J. P. Albert, J. P. Goff, and N. Frenkel.** 1990. Putative site for the acquisition of human herpesvirus 6 virion tegument. J. Virol. **64:**6308–6313.
46. **Roizman, B., and D. M. Knipe.** 2001. Herpes simplex viruses and their replication, p. 2399–2459. *In* B. N. Fields, D. M. Knipe, and P. M. Howley (ed.), Fields virology. Lippincott, Philadelphia, Pa.
47. **Smith, R. F., and T. F. Smith.** 1989. Identification of new protein kinase-related genes in three herpesviruses, herpes simplex virus, varicella-zoster virus, and Epstein-Barr virus. J. Virol. **63:**450–455.
48. **Sommer, M. H., E. Zagha, O. K. Serrano, C. C. Ku, L. Zerboni, A. Baiker, R. Santos, M. Spengler, J. Lynch, C. Grose, W. Ruyechan, J. Hay, and A. M. Arvin.** 2001. Mutational analysis of the repeated open reading frames, ORFs 63 and 70 and ORFs 64 and 69, of varicella-zoster virus. J. Virol. **75:**8224–8239.
49. **Soong, W., J. C. Schultz, A. C. Patera, M. H. Sommer, and J. I. Cohen.** 2000. Infection of human T lymphocytes with varicella-zoster virus: an analysis with viral mutants and clinical isolates. J. Virol. **74:**1864–1870.
50. **Stevenson, D., K. L. Colman, and A. J. Davison.** 1994. Characterization of the putative protein kinases specified by varicella-zoster virus genes 47 and 66. J. Gen. Virol. **75:**317–326.
51. **Takashima, Y., H. Tamura, X. Xuan, and T. Otsuka.** 1999. Identification of the US3 gene product of BHV-1 as a protein kinase and characterization of BHV-1 mutants of the US3 gene. Virus Res. **59:**23–34.
52. **Tuazon, P. T., W. C. Spanos, E. L. Gump, C. A. Monnig, and J. A. Traugh.** 1997. Determinants for substrate phosphorylation by p21-activated protein kinase (γ-PAK). Biochemistry **36:**16059–16064.